

# AMPK improves gut epithelial differentiation and barrier function via regulating *Cdx2* expression

Xiaofei Sun<sup>1,2</sup>, Qiyuan Yang<sup>3</sup>, Carl J Rogers<sup>3</sup>, Min Du<sup>3</sup> and Mei-Jun Zhu<sup>\*1,2</sup>

Impairment in gut epithelial integrity and barrier function is associated with many diseases. The homeostasis of intestinal barrier is based on a delicate regulation of epithelial proliferation and differentiation. AMP-activated protein kinase (AMPK) is a master regulator of energy metabolism, and cellular metabolites are intrinsically involved in epigenetic modifications governing cell differentiation. We aimed to evaluate the regulatory role of AMPK on intestinal epithelial development and barrier function. In this study, AMPK activator (AICAR) improved the barrier function of Caco-2 cells as indicated by increased transepithelial electrical resistance and reduced paracellular FITC-dextran permeability; consistently, AICAR enhanced epithelial differentiation and tight junction formation. Transfection of Caco-2 cells with AMPK WT plasmid, which enhances AMPK activity, improved epithelial barrier function and epithelial differentiation, while K45R (AMPK dominant negative mutant) impaired; these changes were correlated with the expression of caudal type homeobox 2 (CDX2), the key transcription factor committing cells to intestinal epithelial lineage. CDX2 deficiency abolished intestinal differentiation promoted by AMPK activation. Mechanistically, AMPK inactivation was associated with polycomb repressive complex 2 regulated enrichment of H3K27me<sub>3</sub>, the inhibitory histone modification, and lysine-specific histone demethylase-1-mediated reduction of H3K4me<sub>3</sub>, a permissive histone modification. Those histone modifications provide a mechanistic link between AMPK and CDX2 expression. Consistently, epithelial AMPK knockout *in vivo* reduced CDX2 expression, impaired intestinal barrier function, integrity and ultrastructure of tight junction, and epithelial cell migration, promoted intestinal proliferation and exaggerated dextran sulfate sodium-induced colitis. In summary, AMPK enhances intestinal barrier function and epithelial differentiation via promoting CDX2 expression, which is partially mediated by altered histone modifications in the *Cdx2* promoter.

*Cell Death and Differentiation* (2017) 24, 819–831; doi:10.1038/cdd.2017.14; published online 24 February 2017

Intestinal epithelium is responsible for nutrient absorption and defense against harmful microorganisms and lumen contents.<sup>1</sup> Impaired intestinal barrier function is one of the key etiological factors of inflammatory bowel disease (IBD), and other digestive tract diseases.<sup>2</sup> Thus, proper intestinal barrier is essential for health, which requires a delicate regulation of epithelial proliferation and differentiation.<sup>1</sup>

Adenosine monophosphate-activated protein kinase (AMPK) is a heterotrimer; the catalytic  $\alpha$ -subunit of AMPK has two isoforms.<sup>3</sup> AMPK is a master regulator of energy metabolism, and its inactivation was recently discovered as a major etiological factor of many diseases, including obesity and diabetes.<sup>4</sup> Because diabetic and obese mice showed leaky intestinal barrier features,<sup>5</sup> AMPK inhibition due to these conditions may be a key contributor to the impaired gut epithelial differentiation and barrier function. Consistently, the microbial metabolite, butyrate, enhances barrier function and alleviates metabolic syndrome through activation of AMPK.<sup>6</sup> In addition, AMPK is involved in the establishment and maintenance of intestinal polarity and localization of glucose transporters.<sup>7</sup> Up to now, however, the role of AMPK in intestinal epithelial differentiation and colitis onset has not been studied.

Caudal type homeobox 2 (CDX2) is a key transcription factor governing differentiation of intestinal epithelial cells.<sup>8</sup>

Epigenetic modifications are indispensable for transcription initiation, which loosen chromatin structure and allow the binding of RNA polymerase to initiate transcription.<sup>9</sup> Polycomb repressive complex 2 (PRC2), containing the enhancer of zeste homolog 2 (EZH2) catalytic subunit, trimethylates H3K27 (H3K27me<sub>3</sub>) to silence the transcription of target genes.<sup>10</sup> Lysine-specific histone demethylase-1 (LSD1) and lysine demethylase 5 remove H3K4 trimethylation (H3K4me<sub>3</sub>) to inhibit gene transcription.<sup>11</sup> The co-existence of H3K27me<sub>3</sub> and H3K4me<sub>3</sub> in key developmental genes to form a 'bivalent state', which poses the gene to express via enriching H3K4me<sub>3</sub> and reducing H3K27me<sub>3</sub>,<sup>12</sup> though the bivalent state of *Cdx2* gene has not been studied. Recent studies suggest an intrinsic link between metabolism and epigenetic modifications.<sup>13</sup> Drugs altering AMPK activity change histone modifications in J1 ES cells<sup>14</sup> and HepG2 cells.<sup>15</sup> These data prompted us to hypothesize that AMPK promotes epithelial differentiation and enhances epithelial barrier function via epigenetically promoting *Cdx2* expression.

## Results

**AMPK enhances intestinal barrier function through promoting intestinal epithelial differentiation.** To test the

<sup>1</sup>School of Food Science, Washington State University, Pullman 99164, WA, USA; <sup>2</sup>School of Food Science, University of Idaho, Moscow 83844, ID, USA and <sup>3</sup>Department of Animal Science, Washington State University, Pullman 99164, WA, USA

\*Corresponding author: M-J Zhu, School of Food Science, Washington State University, Pullman, WA 99164, USA. Tel: (509) 335 4815; Fax: (509) 335 4815; E-mail: meijun.zhu@wsu.edu

Received 10.7.16; revised 09.1.17; accepted 19.1.17; Edited by R De Maria; published online 24.2.2017

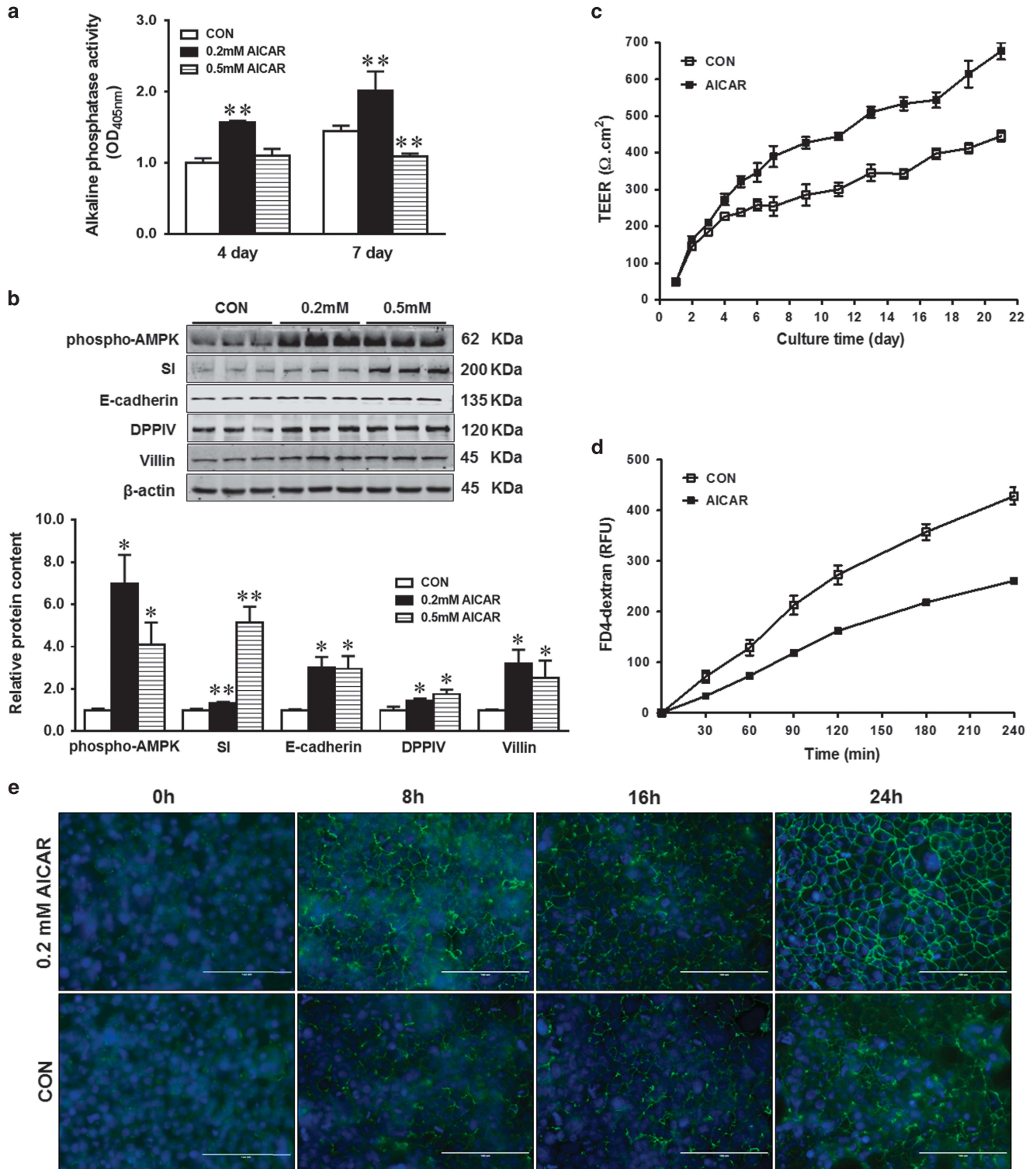


**Figure 1** AICAR treatment enhances differentiation of Caco-2 cells. (a) Alkaline phosphatase activity in Caco-2 cells treated with 0, 0.2 or 0.5 mM AICAR. (b) Enhanced protein content of phospho-AMPK, SI (sucrase-isomaltase), E-cadherin, DPPIV (dipeptidyl peptidase-4) and villin in Caco-2 cells treated with 0.2 or 0.5 mM AICAR. (c) Transepithelial electrical resistance over time. (d) FITC-dextran paracellular intestinal epithelial permeability at 21 days post incubation. (e) Immunofluorescence staining of tight junction protein ZO-1 pre- and post- calcium switch assay. Caco-2 cells were grown to confluence with or without 0.2 mM AICAR and subjected to a calcium switch assay. Cells were fixed at various time points (0, 8, 16 and 24 h) after restoration of Ca<sup>2+</sup> containing medium. Data are representative of three separate experiments. Scale bar is 100 μm. Mean ± S.E.M., n = 4, \*P < 0.05 versus CON; \*\*P < 0.01 versus CON

role of AMPK in gut epithelial function, we used AMPK activator AICAR to activate AMPK in Caco-2 epithelial cells. Both 0.2 and 0.5 mM AICAR activated AMPK (Figure 1b).

Sucrase-isomaltase (SI), E-cadherin, dipeptidyl peptidase-4 (DPPIV) and villin protein levels as well as alkaline phosphatase (AP) activity were increased in response to

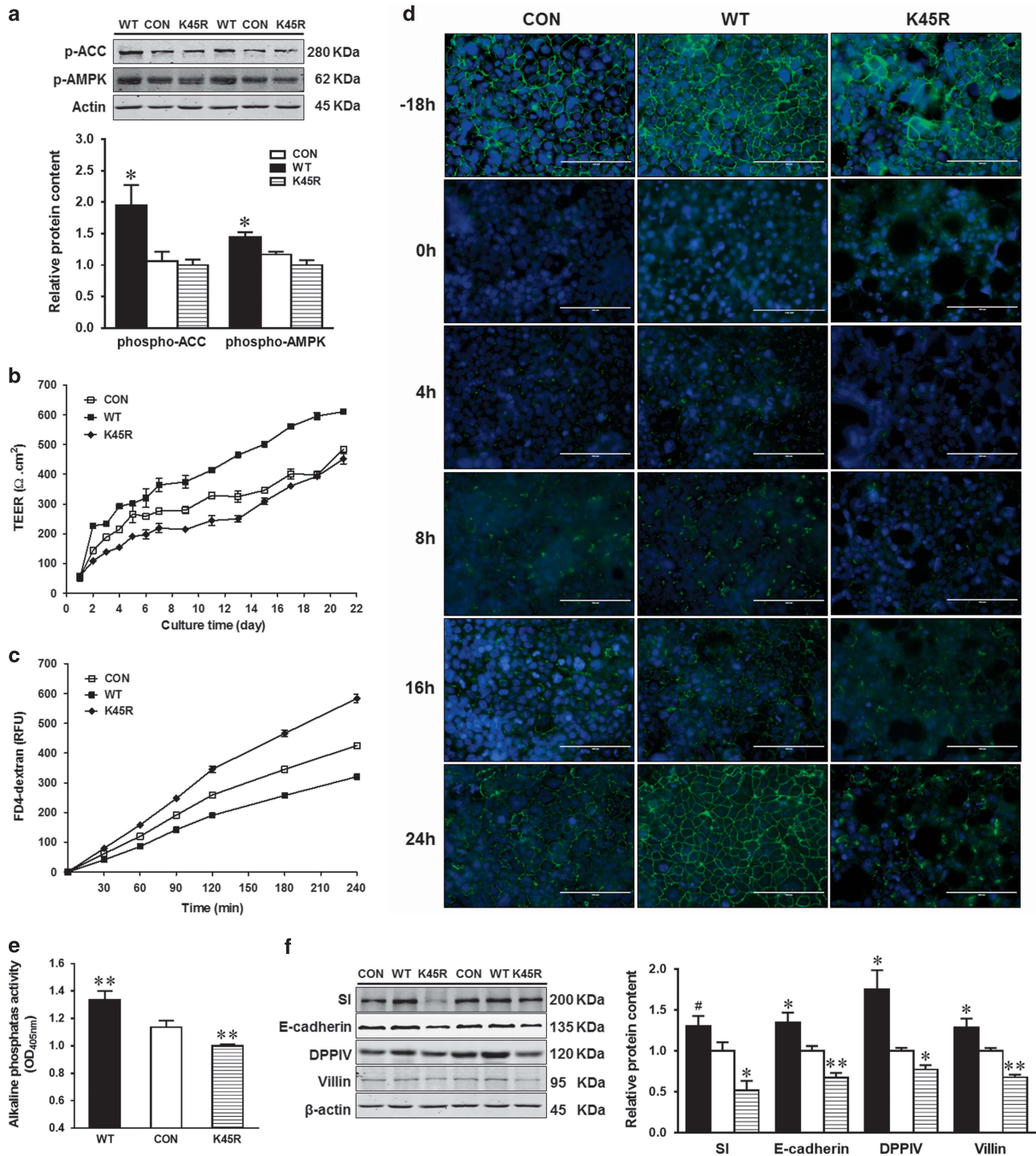


**Figure 2** AMPK promotes intestinal epithelial differentiation. Caco-2 cells were transfected with EGFP (CON), AMPK $\alpha$  WT (WT) or AMPK $\alpha$  K45R (K45R) plasmid. (a) Phospho-ACC and phospho-AMPK activation. (b) Transepithelial electrical resistance over time. (c) FITC-dextran paracellular intestinal epithelial permeability at 21 days post incubation. (d) Immunofluorescent staining of tight junction protein ZO-1 pre- and post-calcium switch assay. Caco-2 cells were grown to confluence and subjected to a calcium switch assay. Cells were fixed 18 h before calcium switch (-18 h) and various time points (0, 4, 8, 16 and 24 h) after restoration of Ca<sup>2+</sup> containing medium. Scale bar is 100  $\mu$ m. (e) Alkaline phosphatase activity. (f) Protein contents of SI (sucrase-isomaltase), E-cadherin, DPPIV (dipeptidyl peptidase-4) and villin. Data are representative of three separate experiments. Mean  $\pm$  S.E.M.,  $n = 4$ , # $P < 0.1$  versus CON, \* $P < 0.05$  versus CON; \*\* $P < 0.01$  versus CON

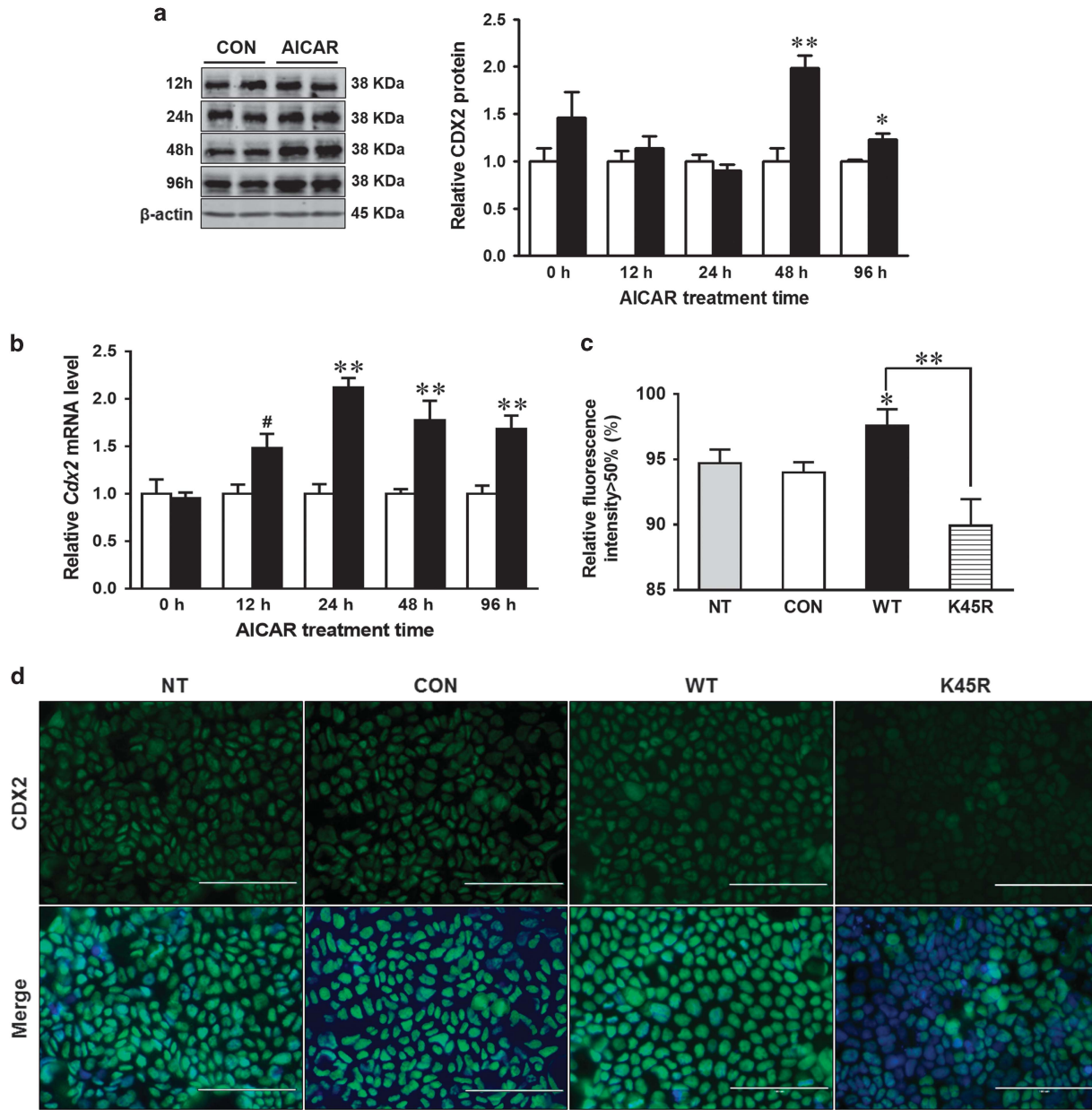


**Figure 3** AMPK enhances CDX2 expression in intestinal epithelial cells. Caco-2 cells were treated with 0 or 0.2 mM AICAR for 96 h when cells were collected for analysis. (a) Protein content of CDX2. (b) mRNA expression of *Cdx2*. (c and d) Immunofluorescent staining of CDX2 in non-transfected (NT) Caco-2 cells, or Caco-2 cells transfected with EGFP (CON), or AMPK $\alpha$  WT (WT) or AMPK $\alpha$  K45R (K45R) plasmid. Scale bar is 100  $\mu$ m. Data are representative of three separate experiments. Mean  $\pm$  S.E.M.,  $n=4$ , <sup>#</sup> $P<0.1$  versus CON; <sup>\*</sup> $P<0.05$  versus CON; <sup>\*\*</sup> $P<0.01$  versus CON

0.2 mM AICAR treatment (Figures 1a and b). However, 0.5 mM AICAR did not change AP activity at 4 days and even decreased its activity after 7 days (Figure 1a). Even though the mechanisms were not understood, as a AMP analog, a high level of AICAR might mimic starvation, which induces a rapid decrease in the expression of intestinal AP, while refeeding resulted in AP upregulation.<sup>16</sup> Associated with AMPK activation and enhanced epithelial differentiation, the epithelial barrier function was improved as shown by increased transepithelial electrical resistance (TEER; Figure 1c) and decreased paracellular permeability of FITC-

dextran (Figure 1d). To assess the reassembly of calcium-induced tight junction, we monitored the relocation of ZO-1 after switching to calcium containing medium. The assembly ability of tight junction in response to calcium switch (Figure 1e) was greatly enhanced by 0.2 mM AICAR treatment. Given that cellular responses to 4 and 7 days of AICAR treatments were similar, 0.2 mM AICAR treatment for 4 days was used in subsequent studies.

Because AICAR is regarded as a nonspecific activator of AMPK due to its ability to activate AMP-dependent enzymes,<sup>17</sup> Caco-2 cells were further transfected with AMPK $\alpha$

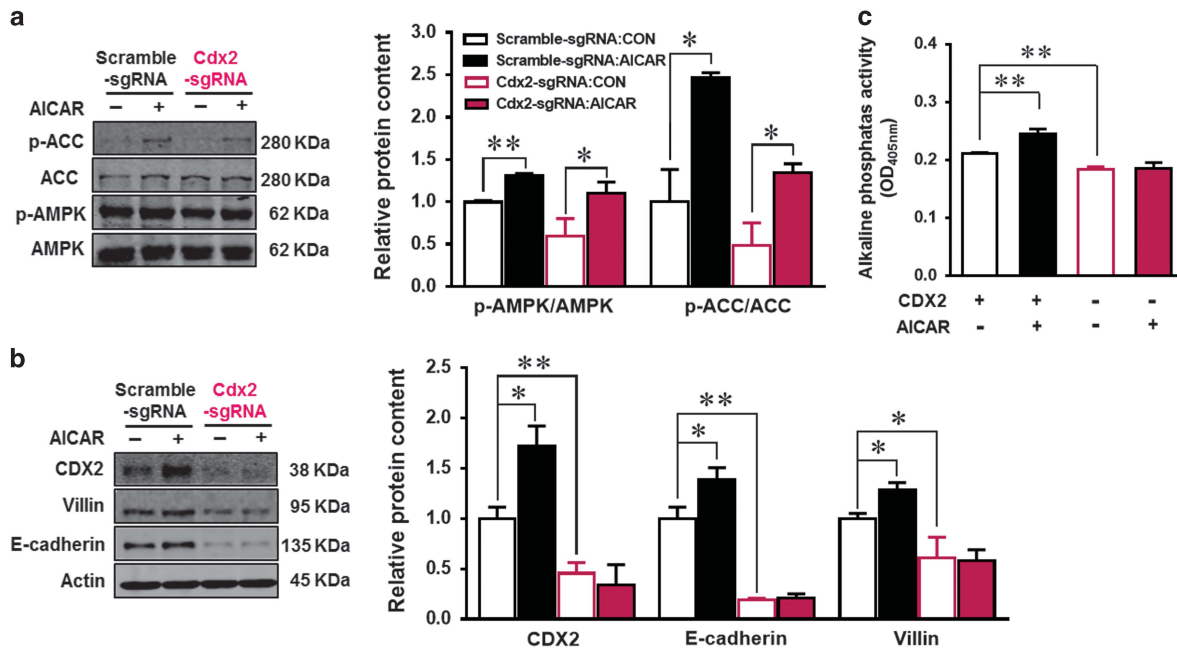


**Figure 4** CDX2 knockout abolishes the positive effects of AICAR on intestinal differentiation. Caco-2 cells were transfected with scrambled CRISPR/Cas9 plasmid (scramble-sgRNA) or CDX2 CRISPR/Cas9 plasmid (Cdx2 sgRNA) to delete Cdx2 or not. Transfected cells with GFP expression (plasmid carries GFP gene) were isolated using cell sorting, then treated with 0 or 0.2 mM AICAR for 4 days. (a) Protein contents of phospho-ACC, ACC, phospho-AMPK and AMPK. (b) Protein contents of CDX2, villin, E-cadherin and beta-actin. (c) Alkaline phosphatase activity. Data are representative of three separate experiments. Mean  $\pm$  S.E.M.,  $n = 3$ , \* $P < 0.05$  versus Scramble-sgRNA; \*\* $P < 0.01$  versus Scramble-sgRNA

WT or K45R plasmid to activate or inhibit AMPK activity. As expected, AMPK signaling was activated in Caco-2 cells transfected with AMPK $\alpha$  WT, as shown by increased levels of phospho-AMPK and phospho-Acetyl-CoA carboxylase (ACC), an exclusive substrate of AMPK (Figure 2a). Consistently, AMPK $\alpha$  WT transfection increased the TEER value (Figure 2b) and reduced paracellular permeability of FITC-dextran (Figure 2c). In line with, the paracellular permeability of FITC-dextran increased in Caco-2 cells transfected with kinase dead AMPK $\alpha$  K45R plasmid compared with cells with CON and AMPK WT plasmids (Figure 2c). We further examined the tight junction protein, zonula occludens 1 (ZO-1), assembly in transfected Caco-2 cells. The fragmented strands of ZO-1 staining at cell borders were formed much faster in AMPK $\alpha$  WT transfected cells compared to AMPK $\alpha$  K45R transfected cells (Figure 2d). Consistently, AP activity and the expression of intestinal differentiation markers (SI, E-cadherin, DPPIV and villin) were enhanced in Caco-2 cells transfected with WT but decreased in cells with K45R when compared to CON (Figures 2e and f).

**AMPK promotes intestinal epithelial differentiation through upregulating CDX2 expression.** CDX2 is the key transcription factor governing epithelial cell differentiation.<sup>8</sup> In response to 0.2 mM AICAR treatment, CDX2 protein content increased after 48 h (Figure 3a). Consistently, *Cdx2* mRNA level was enhanced at 24 h of treatment (Figure 3b). The slightly delayed increase in CDX2 protein content compared to its mRNA expression could be due to the time needed for protein synthesis and post-translational modifications.<sup>18</sup>

Immunofluorescence staining revealed a lower level of CDX2 expression in Caco-2 cells with kinase dead K45R plasmid compared to Caco-2 cells with AMPK WT plasmid (Figures 3c and d).

To further examine the mediatory role of CDX2 in linking AMPK to epithelial differentiation, we used CRISPR/Cas9 system to knockout CDX2. CRISPR/Cas9 system itself showed no effect on Caco-2 cells as indicated by the predicted selectivity of sgRNA (Supplementary Figure S1a and b), and no change in the expression of CDX2 and differentiation markers in cells transfected with scrambled CRISPR/Cas9 plasmid (Supplementary Figure S1c), while CDX2 expression was decreased greatly after CDX2 specific CRISPR/Cas9 transfection and sorting (Figure 4b). 0.2 mM AICAR activated AMPK both in CDX2 control (Scramble-sgRNA) and CDX2 knockout (Cdx2 sgRNA) cells (Figure 4a). Consistently, CDX2 knockout abolished epithelial differentiation enhanced by AICAR as indicated by unchanged AP activity as well as E-cadherin and villin contents in response to AICAR treatment (Figures 4b and c), clearly showing that AMPK-enhanced epithelial differentiation through enhancing CDX2 expression.

**AMPK regulates *Cdx2* expression through inducing histone modifications.** To assess whether the enhanced CDX2 level observed in epithelial cells with AMPK stimulation was due to epigenetic alterations in the *Cdx2* promoter, we further analyzed permissive histone modification H3K4me3 and inhibitory histone modification H3K27me3 based on NCBI ChIP-seq profiles of the *Cdx2* promoter (Figure 5a). H3K4me3 and H3K27me3 are abundant in the *Cdx2*

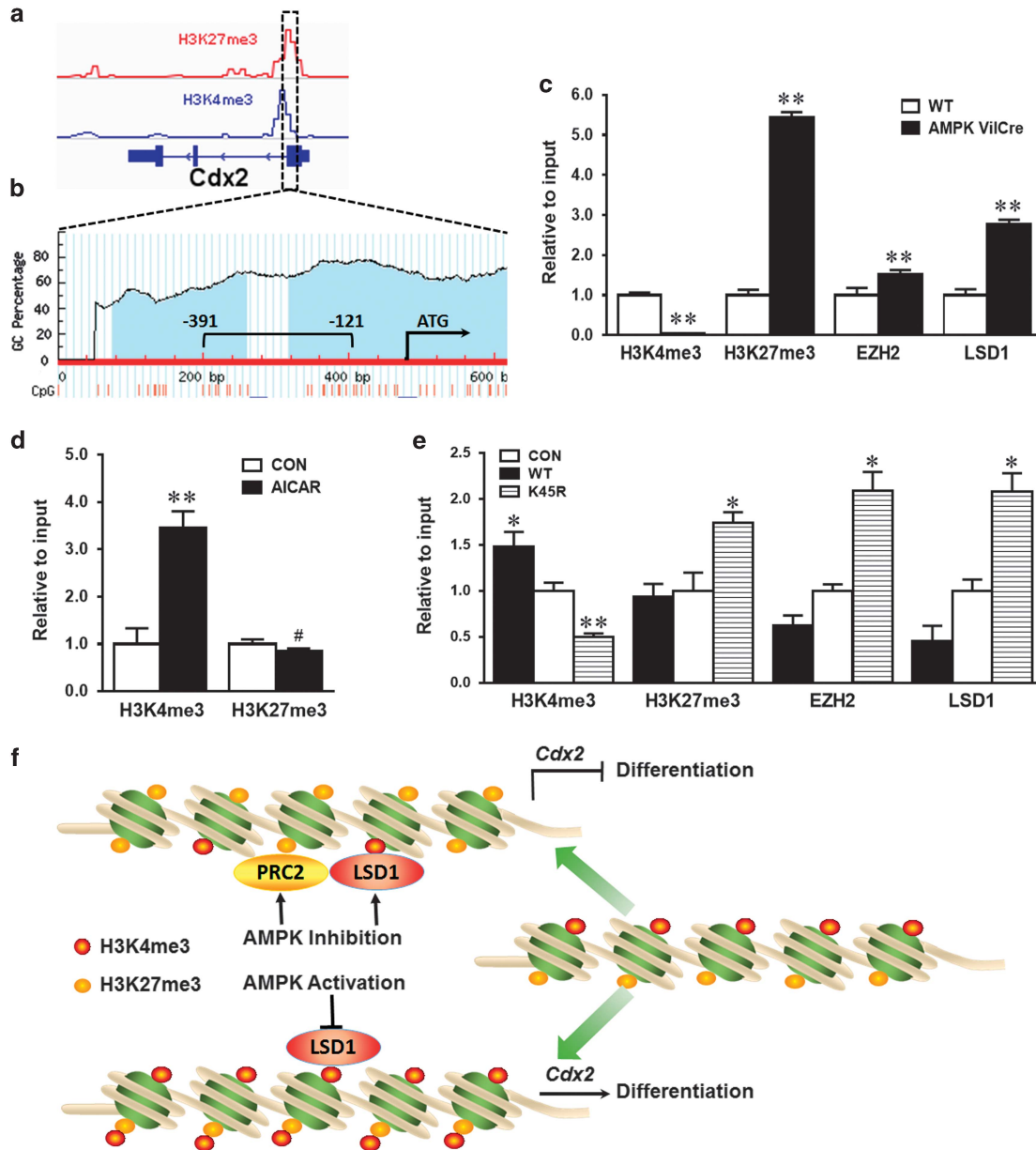


**Figure 5** AMPK regulates *Cdx2* transcription through inducing histone modifications. (a) Data analysis for epigenetic modifications in the *Cdx2* promoter based on NCBI ChIP-Seq profile of H3K4me3 and H3K27me3. (b) CpG sites profile and genomic structure in the *Cdx2* promoter. Blue regions show CpG islands. Red lines show CpG dinucleotides. -391 bp to -121 bp represents primer amplification region. (c) H3K4me3 and H3K27me3 modifications as well as binding status of EZH2 and LSD1 in the *Cdx2* promoter of AMPK ViCre KO and WT mice using ChIP-PCR. (d) H3K4me3 and H3K27me3 modifications in the *Cdx2* promoter of Caco-2 cells treated with or without 0.2 mM AICAR and measured by ChIP-PCR. (e) H3K4me3 and H3K27me3 modifications as well as binding status of EZH2 and LSD1 in the *Cdx2* promoter of Caco-2 cells transfected with EGFP (CON), AMPK $\alpha$  WT (WT) or AMPK $\alpha$  K45R (K45R) plasmid. (f) A proposed model for the effects of AMPK on intestinal differentiation via inducing histone modifications by regulating methylase and demethylase in the *Cdx2* promoter. Data are representative of three separate experiments. Mean  $\pm$  S.E.M.;  $n=3$ , # $P<0.1$  versus CON; \* $P<0.05$  versus CON; \*\* $P<0.05$  versus CON

promoter, making it into a bivalent state, which keeps the gene in a poised status. We further analyzed the abundance of CpG islands in the *Cdx2* promoter. As expected, exceptionally rich CpG sites in the *Cdx2* promoter were found (Figure 5b), consistent with the characteristics of bivalent key developmental genes. To test whether AMPK alters the bivalent state of *Cdx2* promoter to regulate its expression, we further used chromatin immunoprecipitation (ChIP) of H3K4me3 and H3K27me3 followed by PCR using

primers specific to the *Cdx2* promoter. AMPK deletion *in vivo* dramatically decreased H3K4me3 and increased H3K27me3 contents (Figure 5c). *In vitro*, AICAR treatment increased H3K4me3 but not H3K27me3 in the promoter of *Cdx2* gene (Figure 5d). In alignment, H3K4me3 was enriched while H3K27me3 was reduced in cells transfected with AMPK $\alpha$  WT plasmid compared to those with kinase dead K45R plasmid (Figure 5e). PRC2 bears histone methyltransferase activity on H3K27me3, while LSD1 is a histone demethylase for

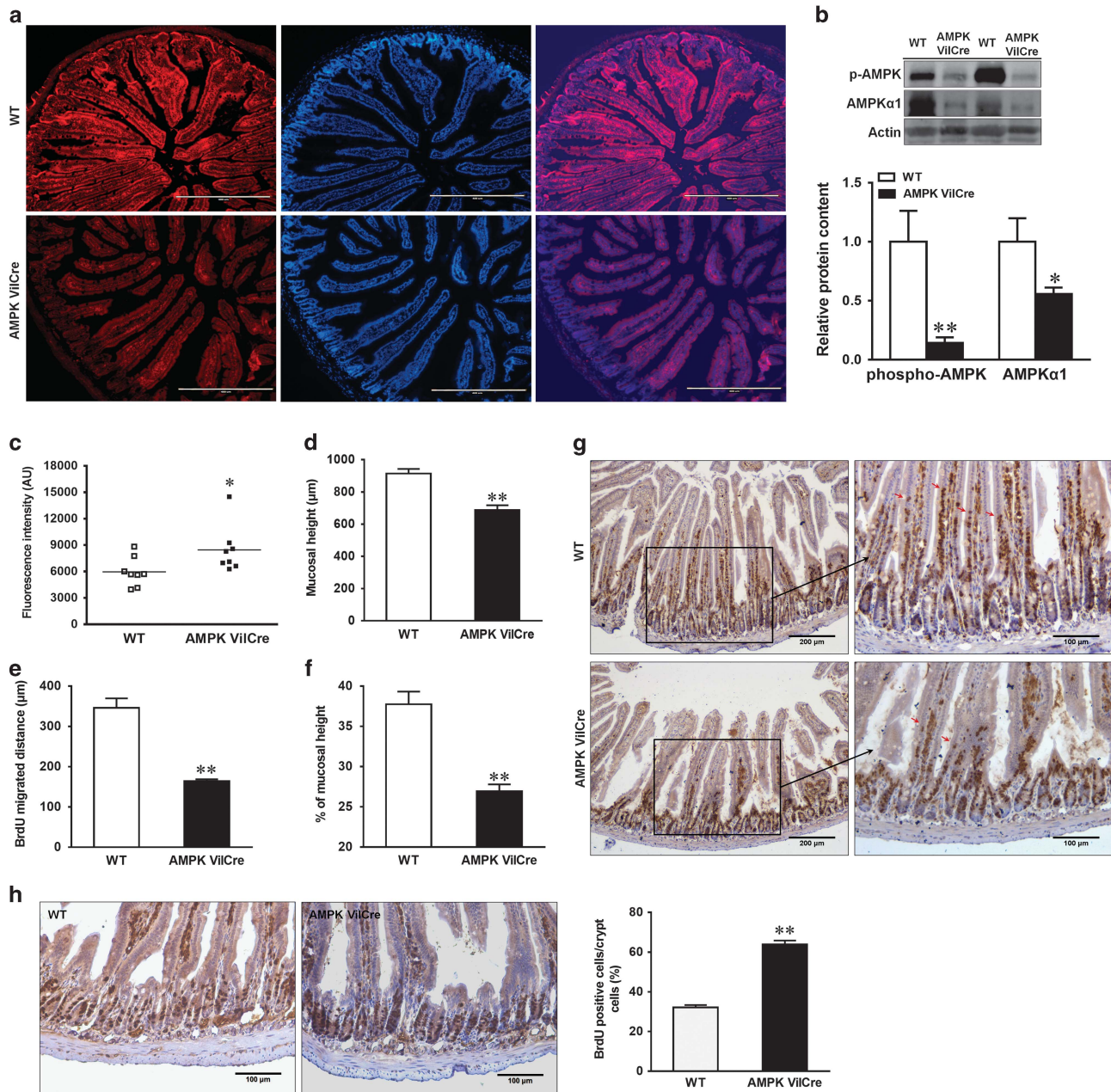
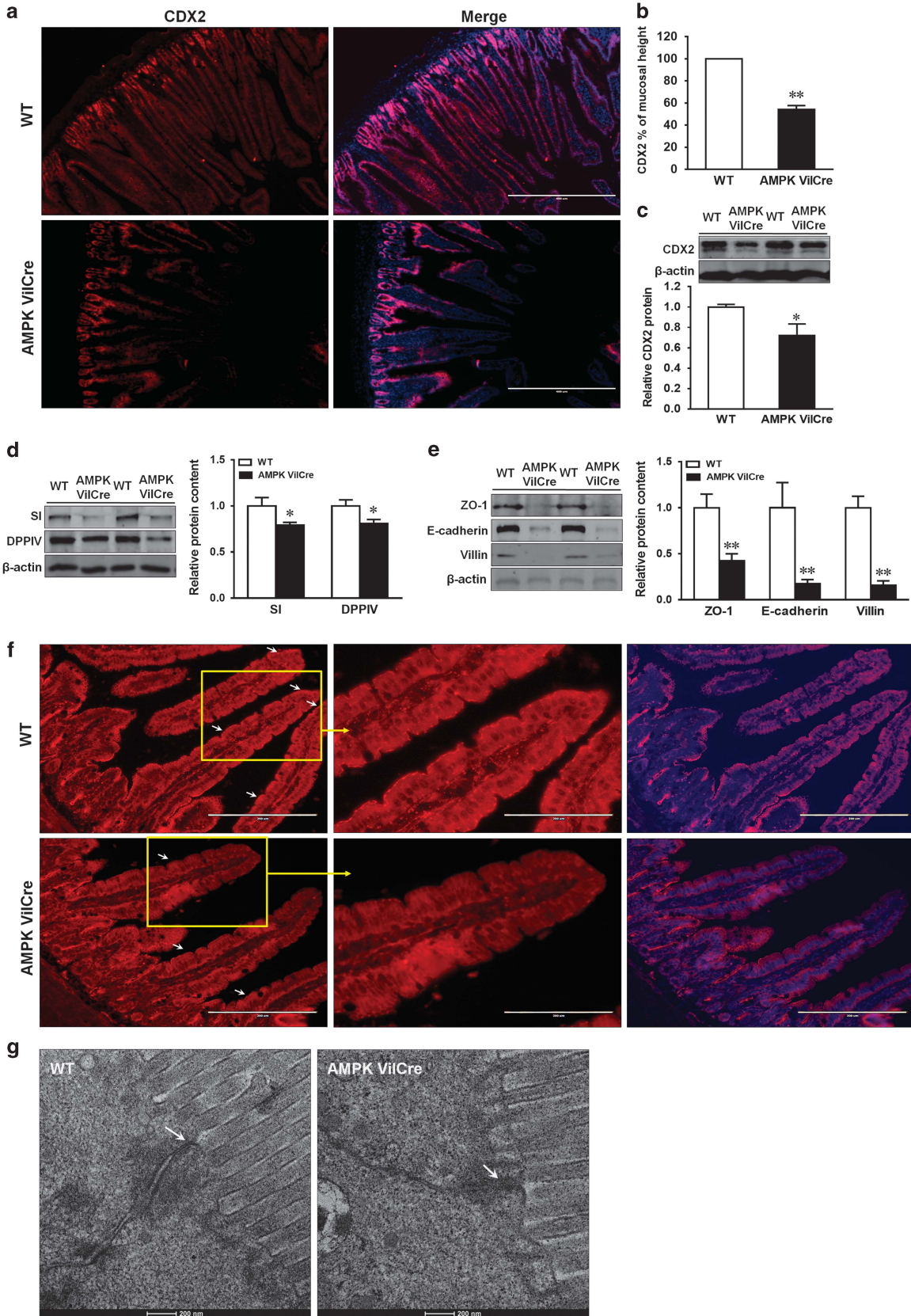


**Figure 6** AMPK enhances intestinal barrier function and migration, and alters proliferation *in vivo*. Jejunum tissues of AMPK ViiCre KO and WT male mice (2.5 months of age) were used. **(a)** Immunofluorescent staining of phospho-AMPK. Scale bars represent 400  $\mu$ m. **(b)** Protein contents of phospho-AMPK and AMPK $\alpha$ 1. **(c)** *In vivo* paracellular intestinal epithelial permeability of FITC-dextran. **(d)** Mucosal height. **(e)** Enterocyte migration. **(f)** Enterocyte migration relative to mucosal height. **(g)** 24 h post a single BrdU injection for intestinal migration staining. Arrows indicate the farthest BrdU-positive enterocytes. Scale bars represent 200  $\mu$ m on the left and 100  $\mu$ m on the right. **(h)** 2 h post a single BrdU injection for intestinal proliferation analysis. Scale bars represent 100  $\mu$ m. Data are representative of three separate experiments. Mean  $\pm$  S.E.M.;  $n = 8$ , \* $P < 0.05$  versus WT; \*\* $P < 0.01$  versus WT

H3K4me1/2. To further explore the underlying mechanism, EZH2 and LSD1 binding to the *Cdx2* promoter were analyzed by ChIP. Consistent with reduced H3K4me3 and enriched H3K27me3, EZH2 and LSD1 were recruited to the *Cdx2* promoter after AMPK knock out (Figures 5c and e). These data indicated that AMPK regulates *Cdx2* expression at least partially through inducing histone modifications by recruiting methylase PRC2 and demethylase LSD1 to the *Cdx2* promoter (Figure 5f).

**AMPK deletion reduces CDX2 expression, impairs barrier function and exacerbates colitis *in vivo*.** To assess the regulatory role of AMPK in intestinal epithelium *in vivo*, we cross-bred AMPK $\alpha$ 1-floxed mice with ViiCre mice to specifically knock out AMPK $\alpha$ 1 gene in intestinal epithelial cells where villin is expressed. AMPK was efficiently deleted in the gut epithelium of AMPK ViiCre mice, as indicated by immunofluorescence staining (Figure 6a) and dramatically decreased phospho-AMPK and AMPK $\alpha$ 1 ratio (Figure 6b).





AMPK *VilCre* mice had increased FITC-dextran in their serum compared with WT mice, showing a leaking gut (Figure 6c). Furthermore, mucosal height (Figure 6d) and the migration of 24 h BrdU-labeled enterocytes (Figures 6e-g) were decreased in AMPK *VilCre* mice compared to WT mice. In addition, the proliferation of 2 h BrdU-labeled progenitor cells was enhanced in AMPK *VilCre* mice (Figure 6h).

We further examined the expression pattern of CDX2 in WT and AMPK *VilCre* mice. CDX2 in WT mice resided along the epithelial cells from crypts to the most of villi, whereas CDX2 in AMPK *VilCre* extended from crypt to the middle of villi (Figures 7a and b). Consistently, the protein content of CDX2 was reduced in AMPK *VilCre* mice (Figure 7c). Consequently, the brush border enzyme, SI and DPPIV, were abated in AMPK *VilCre* mice (Figure 7d). Similarly, the contents of intestinal junctions, such as ZO-1 and E-cadherin, and villin were diminished (Figure 7e). To investigate the integrity of tight junctions, ZO-1 immunofluorescence staining was analyzed. The pattern of ZO-1 at the tip of villi was impaired in jejunum tissue of AMPK *VilCre* mice (Figure 7f), which was in alignment with CDX2 pattern (Figure 7a). To examine the ultrastructure of tight junctions, transmission electron microscopy (TEM) was further conducted. The intercellular tight junctions appeared to be denser in WT mice than that in AMPK *VilCre* mice (Figure 7g).

To demonstrate the clinical importance, we next examined colitis susceptibility of these mice upon dextran sulfate sodium

(DSS) induction. Epithelial specific AMPK deletion in mice resulted in increased disease activity index (DAI) scores, watery and bloody diarrhea, and dramatic body weight loss in response to DSS challenge (Figure 8a). Furthermore, AMPK *VilCre* mice had significantly higher histopathological scores compared to WT mice (Figure 8b), suggesting AMPK deletion exacerbated colitis. In addition, AMPK mice display mortality during colitis induction; one mouse was died in AMPK *VilCre* group during DSS treatment while all mice in WT group survived DSS challenge.

## Discussion

Gut epithelium forms the largest and critical barrier against the external environment, which is constantly renewed.<sup>19</sup> During intestinal epithelial development, enterocytes migrate from the crypt base to villi while differentiate into enterocytes, goblet cells and enteroendocrine cells.<sup>20</sup> The balance of epithelial proliferation, differentiation and migration is critical for epithelial health.<sup>21</sup> Impairment in gut epithelial integrity and barrier function, so called 'leaky gut' is a central etiological factor for IBD. In this study, AMPK villin specific deletion deteriorated DSS-induced colitis, indicating AMPK might be a key mediator involved in the etiology of IBD. Similarly, the administration of AMPK activator, AICAR, attenuated 2,4,6-trinitrobenzene sulfonic acid (TNBS)-induced acute and relapsing colitis.<sup>22</sup> This ameliorative effects of AMPK on IBD likely result from

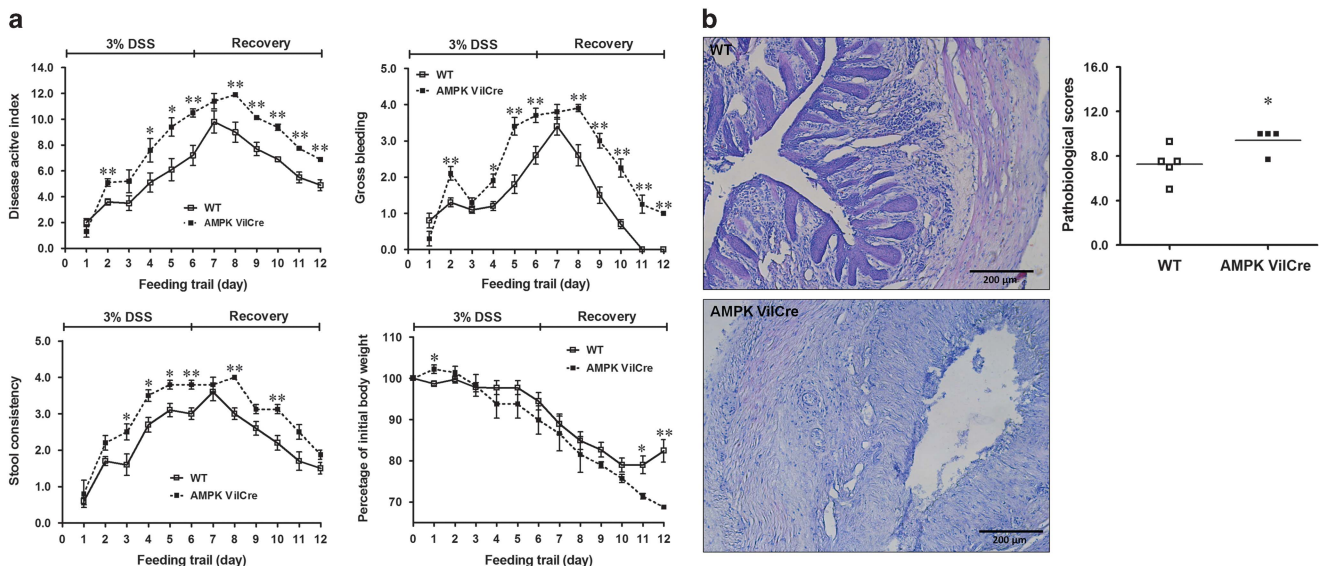


**Figure 8** AMPK deletion exacerbates DSS-induced colitis. AMPK *VilCre* KO and WT male mice (3 months of age) were induced colitis by 3% DSS for 6 days, followed by 6 days of recovery. (a) Disease activity index including body weight, gross bleeding and stool consistency were monitored and scored daily. (b) Pathological scores in DSS-induced distal colon. Scale bars are 200  $\mu$ m. Mean  $\pm$  S.E.M.;  $n=5$ , \* $P<0.05$  versus WT; \*\* $P<0.01$  versus WT

**Figure 7** AMPK knockout decreases CDX2 content and intestinal differentiation *in vivo*. Jejunum tissues of AMPK *VilCre* KO and WT male mice (2.5 months of age) were used. (a) Immunofluorescent staining of CDX2. Scale bar is 400  $\mu$ m. (b) CDX2 staining relative to mucosal height. (c) Protein content of CDX2. (d) Protein content of SI (sucrase-isomaltase) and DPPIV (dipeptidyl peptidase-4). (e) Protein content of ZO-1, E-cadherin and villin. (f) Immunofluorescent staining of ZO-1 in jejunum tissues. Arrows indicate ZO-1 at the border of villus. Scale bar is 200  $\mu$ m. (g) Transmission electron microscopy (TEM) ultrastructure of tight junction. Arrows indicate tight junctions. Scale bar is 200 nm. Mean  $\pm$  S.E.M.;  $n=8$ , \* $P<0.05$  versus WT; \*\* $P<0.01$  versus WT

improved epithelial barrier function. Besides in IBD, abnormal intestinal barrier function was one of the key causes of metabolic disorders. Disrupted epithelial barrier function is associated with obesity and diabetes.<sup>23</sup> In addition, a number of diseases and pathophysiological states such as obesity caused by high fat diet and sedentary life style are associated with attenuation of AMPK activity;<sup>24</sup> AMPK activation by AICAR or exercise mitigates symptoms associated with these conditions.<sup>4</sup> Metformin, a most commonly used therapeutic drug for diabetes and obesity, activates AMPK, having beneficial effects on fructose-induced loss of tight junction in duodenum.<sup>25</sup> Using IL-10 KO mice, we found that metformin supplementation improved intestinal epithelial barrier function associated with enhanced AMPK activation in ileum.<sup>26</sup> Therefore, AMPK exhibits crucial roles in mitigating IBD, and metabolic disorders-induced bowel dysfunctions, which might be partially caused by abnormal intestinal barrier function. However, the underlying connection and crosstalk between metabolic sensor and intestinal barrier function have only been sparsely studied. This study examined the role of AMPK in mediating intestinal epithelial barrier function and further explored underlying mechanisms.

AMPK contains one catalytic  $\alpha$ -subunit, which has two isoforms,  $\alpha 1$  and  $\alpha 2$ . AMPK  $\alpha 1$  is mainly expressed in intestinal epithelial cells,<sup>27</sup> thus its role in epithelial differentiation was examined in the current study. As an important regulator of energy metabolism, AMPK activation or inhibition due to chemicals or pathophysiological states results in complicate changes in the whole body. To clearly define the role of AMPK in epithelial differentiation, we specifically knocked out AMPK $\alpha 1$  gene in epithelial cells expressing villin *in vivo*. Deletion of AMPK in epithelial cells augmented *in vivo* intestinal permeability. This is consistent with a previous study showing AMPK inactivation in obese mice was associated with barrier dysfunction.<sup>28</sup> However, in IL-10 KO mice, where severe inflammation occurs due to the absence of a key anti-inflammatory cytokine, AMPK activation was associated with impairment of gut epithelial barrier function.<sup>29</sup> Such AMPK activation could be due to the impairment in energetic metabolism elicited by inflammation.<sup>30</sup>

Caco-2 cells differentiate after confluence, resembling epithelial differentiation *in vivo*, which have been widely used for studying intestinal barrier function *in vitro*.<sup>6</sup> AICAR, the AMPK activator, can be transported into cells and converted into AMP analog.<sup>31</sup> AICAR promotes TEER in MDCK cells and Caco-2 cells,<sup>32</sup> while compound C that inhibits AMPK activity abolishes intestinal barrier function.<sup>6</sup> Consistent with previous reports, AICAR treatment enhances barrier function and epithelial differentiation in Caco-2 cells. ZO-1 is a critical component of the tight junction complex.<sup>33</sup> In line with improved barrier function, AICAR accelerates the assembly of tight junction. In support, butyrate, which activates AMPK, promotes ZO-1 re-localization and tightens intestinal barrier.<sup>6</sup> These studies demonstrate the regulatory role of AMPK on epithelial differentiation and barrier function. However, in addition to activate AMPK, AICAR also activates other AMP-dependent enzymes, which may complicate interpretation of results.<sup>17</sup> To avoid these complications, Caco-2 cells were further transfected with AMPK WT and kinase dead K45R plasmids. Consistently, Caco-2 cells transfected with AMPK

WT plasmid had enhanced epithelial differentiation, tight junction assembly and improved barrier function, while cells with AMPK kinase dead K45R plasmid had opposite phenomena. Of note, the TEER of AMPK K45R gradually caught up with that of control Caco-2 cells transfected with GFP over time, which was likely due to gradual loss of transfected plasmids in cultured cells. These data in combination clearly show that AMPK is an effective pharmacological target for enhancing intestinal epithelial differentiation and barrier function.

CDX2 is the key transcription factor regulating epithelial differentiation, which primarily expresses in less differentiated epithelial cells.<sup>34</sup> A previous study showed that CDX2 expression presented a vertical gradient with less expression at the tips of the villi.<sup>34</sup> CDX2 overexpression promotes differentiation of HT-29 cells and IEC-6 cells,<sup>35</sup> while CDX2 deficiency impairs enterocyte apical/basolateral polarity and morphogenesis.<sup>36</sup> In the jejunum of AMPK VillCre mice, we found that CDX2 was limited to the lower and mid-villi, which may lead to reduced mucosal height, migration ability and tight junction formation. We further found that CDX2 expression was greatly enhanced in Caco-2 cells with enhanced AMPK activity, which was associated with improved barrier function and differentiation, while CDX2 deletion inhibited epithelial differentiation. In support of our observations, AICAR promotes CDX2 activity in mammalian embryonic development, while compound C inhibits.<sup>37</sup> These data show that AICAR promotes intestinal differentiation directly via upregulation of CDX2. On the other hand, CDX2 is considered as a tumor suppressor,<sup>38</sup> playing a crucial role in inhibiting proliferation.<sup>39</sup> We found proliferation was enhanced in AMPK VillCre mice, which might be partially through inhibiting CDX2. In support, the cell proliferation and cyclin D1 expression were decreased after CDX2 is induced in human intestinal epithelial crypt (HIEC) cells.<sup>40</sup>

Histone modifications regulate gene expression. As a key developmental gene, the promoter of *Cdx2* is enriched with both H3K27me3 and H3K4me3, forming a 'bivalent state'.<sup>41</sup> Our data showed that AMPK activation facilitates permissive H3K4me3 and impedes inhibitory H3K27me3 modification in the *Cdx2* promoter, explaining the enhanced *Cdx2* expression due to AMPK activation. Furthermore, EZH2, the enzymatic component of PRC2, is one of PcG proteins that catalyzes trimethylation of H3K27.<sup>42</sup> In embryonic stem cells, PRC2 works with PRC1 to repress the *Cdx2* expression.<sup>43</sup> LSD1 is the demethylase for H3K4me1/2.<sup>44</sup> In trophoblast stem cells, deletion of LSD1 in mice promotes the expression of *Cdx2*.<sup>45</sup> In agreement with its functionalities and decreased *Cdx2* expression in AMPK WT transfected cells, the deletion of AMPK led to increased EZH2 and LSD1 recruitment in the *Cdx2* promoter.

In summary, for the first time, we found that AMPK strengthens intestinal barrier function and intestinal differentiation through enhancing the expression of *Cdx2*, which is associated with the enhanced formation of permissive histone modification in the *Cdx2* promoter, and decreased binding of PRC2 and LSD1 to the *Cdx2* promoter. *In vivo* mice study demonstrated that AMPK deficiency in intestinal epithelial resulted in exaggerated DSS-induced colitis, a commonly used IBD model. These data deepen the current

understanding about the link between the intracellular energy sensor, AMPK and intestinal epithelial differentiation. Our finding is important because AMPK activity is altered due to a number of pathophysiological conditions such as obesity, diabetes and inflammation, which is known to impair epithelial barrier function. Thus, AMPK provides an ideal drug target for improving gut epithelial health. The translational value of our finding is highlighted by the wide availability of drugs activating AMPK such as the popular antidiabetic drug, metformin, which can be used to improve gut epithelial health.

## Materials and Methods

**Mice strains.** C57BL/6J mice were purchased from Jackson Laboratory (Bar Harbor, ME, USA). Mice with AMPK $\alpha$ 1-floxed gene (Prkaa1<sup>tm1.1Sj</sup>/J, Stock#: 014141, Jackson Lab) were cross-bred with VillCre mice (B6.Cg-Tg<sup>Vil-cre</sup> 997Gum/J, Stock#: 004586, Jackson Lab) to obtain AMPK $\alpha$ 1 villin specific KO (AMPK VillCre) mice. Eight AMPK VillCre male mice and eight wild type (WT) male mice were killed at two and half months of age for epithelial permeability and epithelial cell migration assays. In addition, eight AMPK VillCre and eight WT mice were euthanized at two and half months of age for proliferation assays. Five AMPK VillCre male mice and five WT male mice were killed at three and half months of age for DSS-induced colitis. All studies were performed in an approved protocol by the Institutional Animal Care and Use Committee (IACUC) at Washington State University.

**In vivo permeability, migration and proliferation assays.** Intestinal permeability to FITC-dextran 40 *in vivo* was carried out as previously described with modifications.<sup>46</sup> Briefly, mice were fasted for five hours and orally gavaged with 500 mg/kg body weight FITC-dextran (Sigma, St. Louis, MO, USA). Serum was collected 4 h after gavage and diluted 1:5 with PBS, pH7.4. The fluorescent intensity of each sample was measured on the Synergy H1 microplate fluorescence reader (BioTek, Winooski, VT, USA).

To assess epithelial migration, mice were injected with 100  $\mu$ l of BrdU (10 mg/ml in saline, i.p.) (BD Pharmingen, San Jose, CA, USA) at 24 h prior to sacrifice.<sup>47</sup> To assess epithelial proliferation, another set of mice were injected with BrdU at 2 h prior to sacrifice. At necropsy, a small section of jejunum tissues was frozen in OCT medium for cryo-section preparation and immunostaining. For migration, the distance of foremost BrdU-positive cells to the bottom of crypts indicates the extent of epithelial migration. The mucosal height was measured from crypt base to villus tip. Five sections per mouse were assessed in a blind manner. For proliferation, the percentage of BrdU-positive cells relative to total cell number per crypt was quantified. Three crypts per section, and three sections per mouse were assessed in a blind fashion.

**DSS-induced colitis.** Colitis was induced by 3% (w/v) dextran sulfate sodium (DSS, Millipore Corporation, Billerica, MA, USA) in drinking water for 6 days, and followed by a recovery period of 6 days. The disease activity index (DAI) scores including body weight, gross bleeding and stool consistency were monitored daily.<sup>48</sup> Each parameter of DAI was scored from 0 to 4. The body weight was scored as 0, 1, 2, 3 and 4 when weight loss was <1%, 1–5%, 5–10%, 10–20% and >20%, respectively. The gross bleeding was scored as 0, 1, 2, 3 and 4 when there was no bleeding, no visible blood but stool color changed, small area visible blood, large area visible blood and gross blood on most stool. The stool consistency was scored as 0, 1, 2, 3 and 4 when the stool was firm, soft but could pick up, could not pick up but had shape, could not pick up without shape and watery, respectively.

**Cell culture.** Caco-2 cell line was purchased from American Type Culture Collection (Manassas, VA, USA) and grown at 37 °C with 5% CO<sub>2</sub> in a humidified incubator in DMEM (Sigma) supplemented with 10% fetal bovine serum (GE, Fairfield, CT, USA) and 1% penicillin–streptomycin (Life Technologies, Grand Island, NY, USA). Unless specified, the medium was refreshed every 48 h.

For AICAR treatment, Caco-2 cells were seeded at a density of  $2 \times 10^5$  per well on 12-well plates, and treated with 0, 0.2 or 0.5 mM of 5-aminoimidazole-4-carboxamide riboside (AICAR; Toronto Research Chemical Inc., Ontario, Canada) for 0, 12, 24, 48, and 96 h (for immunoblotting assay and mRNA assay) as well as 4 days (for alkaline phosphatase assay, immunoblotting assay and immunofluorescent staining), 7 days (for alkaline phosphatase assay) and 21 days (for *in vitro* barrier function assessment). Medium was refreshed every day.

For plasmid transfection, Caco-2 cells were transfected with plasmids using Lipofectamine 3000 (Life Technologies) per manufacturer's instructions. Caco-2 cells at 70% confluence were transfected with plasmid constructs containing pAMPK $\alpha$  WT (WT), pAMPK $\alpha$  K45R mutant (K45R), and green fluorescent protein (GFP; CON; Catalog no. 15991, 15992 and 13031; Addgene, Cambridge, MA, USA) using a 2 : 4 : 4 ratio of DNA ( $\mu$ g): lipofectamine ( $\mu$ l): lipofectamine 3000 ( $\mu$ l). Medium was changed 12 h post transfection, when 400  $\mu$ g/ml G418 (Amresco, Solon, OH, USA) was added to the transfected cells for 7 days to enrich cells with transfection. Then the transfected cells were seeded onto 12-well plates at  $2 \times 10^5$  cells per well for 4 days (for alkaline phosphatase assay and immunoblotting assay), 7 days (for alkaline phosphatase assay) and 21 days (for *in vitro* barrier function assessment). Medium was refreshed every day.

The pX330 CRISPR/Cas9 plasmids with *Cdx2* sgRNA (CDX2 knockout) and corresponding random sequences (Scramble-sgRNA) were designed and purchased from Genescript (Piscataway, NJ, USA). Caco-2 cells were transfected with a *Cdx2* sgRNA plasmid or a Scramble-sgRNA plasmid. Three days later, transfected cells with GFP expression (plasmid carries GFP gene) were isolated using FACSaria (BD bioscience, San Jose, CA, USA). Sorted cells were cultured in plates, then seeded onto 12-well plates at  $2 \times 10^5$  cells per well, and treated with 0.2 mM AICAR for 4 days. Medium was refreshed every day.

**Alkaline phosphatase assay.** Alkaline phosphatase (AP) assay was performed as previously described.<sup>16</sup> Briefly, Caco-2 cells were seeded onto 12-well plates at  $2 \times 10^5$  cells per well for 4 days or 7 days, rinsed with PBS, lysed and collected for AP activity measurement. Alkaline phosphatase was assayed by incubating with substrate, pNPP (Sigma), at 37 °C for 30 min. The reaction was stopped with 3 mM NaOH. The absorbance at 405 nm was measured using Synergy H1 microplate reader.

**Immunoblotting analysis.** Immunoblotting analysis was performed according to the procedures as previously described.<sup>49</sup> Membranes were visualized using an Odyssey Infrared Imaging System (Li-Cor Biosciences, Lincoln, NE, USA). Band density was normalized to  $\beta$ -actin. Antibodies against phospho-AMPK at Thr 172, phospho-ACC at Ser 79, AMPK  $\alpha$ 1, villin, DPPIV and CDX2 were purchased from Cell Signaling Technology (Danvers, MA, USA). Anti-E-cadherin antibody and anti-ZO-1 antibody were purchased from Life Technologies. Anti-sucrase-isomaltase antibody and anti- $\beta$ -actin were purchased from DSHB (Iowa, IA, USA). IRDye 680 goat anti-mouse secondary antibody and IRDye 800CW goat anti-rabbit secondary antibody were purchased from Li-Cor Biosciences (Lincoln, NE, USA).

**In vitro barrier function assessment.** Twelve-well plate Millicells (0.4  $\mu$ m, Millipore Corporation) were used for transepithelial electrical resistance (TEER) assays as described previously.<sup>50</sup> Briefly, 0.5 ml Caco-2 cells at the density of  $4 \times 10^5$  cells/ml were seeded in the apical chamber that bathed in the basal chamber with 1.0 ml DMEM complete medium for 21 days. Voltage was measured daily using EVOM (WPI, Sarasota, FL, USA), which was multiplied by the area of filter (1.12 cm<sup>2</sup>) to obtain the TEER in Ohm cm<sup>2</sup>. DMEM complete medium in apical and basal chamber was refreshed every day.

The permeability of FITC-dextran (Sigma) across the Caco-2 cell monolayer was measured as previously described with modifications.<sup>51</sup> At 21 days, 1.0 mg/ml FITC-dextran was added on the apical side of monolayers after being washed twice with PBS. One milliliter sample in the basal chamber was taken at 30, 60, 90, 120, 180 and 240 min, respectively, and 1.0 ml pre-warmed fresh medium was added after each sampling to replenish basal medium. The fluorescence emission at 520 nm was measured with excitation at 490 nm using Synergy H1 microplate reader.

**Immunohistochemistry and histopathology.** Caco-2 cells were fixed in ice-cold methanol for 10 min, blocked in 5% goat serum at room temperature for 1 h, and incubated with anti-ZO-1 (1:200) or anti-CDX2 (1:200) antibody overnight at 4 °C. Stained cells were then incubated with fluorescent secondary antibody (1:1000) at room temperature for 1 h. Goat anti-rabbit Alexa Fluor 488 and goat anti-mouse Alexa Fluor 555 were purchased from Cell Signaling Technology. Fluorescence was examined using EVOS FL fluorescence microscope (Life Technologies) as previously described.<sup>52</sup> Cryosections of mouse jejunum tissue were blocked with 5% goat serum for 1 h, incubated overnight with anti-BrdU antibody, anti-CDX2 antibody, anti-phospho-AMPK at Thr 172 or anti-ZO-1 at 4 °C. An ABC kit (Vector Laboratories, Burlingame, CA, USA) and DAB substrates (Vector Laboratories) were used for BrdU, followed by hematoxylin counterstaining. Immunoreactive sites were visualized by using either fluorescence microscope or

Leica DM2000 LED light microscope (Wetzlar, Germany). The pathology was scored in a blinded manner including severity of inflammation, depth of injury and crypt damage by hematoxylin and eosin stain (H&E stain) as previously reported.<sup>53</sup> The severity of inflammation was scored as 0, 1, 2, 3 when the inflammation is none, slight, moderate and severe, respectively. The depth of injury was scored as 0, 1, 2, 3 when the injury was none, at mucosal, at mucosal and submucosal region, and at transmural region, respectively. The crypt damage was scored as 0, 1, 2, 3, 4 when the damage was none, about 1/3 crypt, about 2/3 crypt, about whole crypt and inducing complete loss of crypt, respectively.

**Calcium switch assay.** The analysis was conducted as previously described with calcium-free DMEM.<sup>54</sup> Briefly, Caco-2 cells were seeded onto 12-well plates at  $2 \times 10^5$  cells per well and grown for 4 days, rinsed with PBS and cultured with calcium-free DMEM for 16 h before being switched back to regular DMEM with calcium. Cells were fixed in ice-cold methanol for 18 h before calcium switch (–18 h) and various time points (0, 4, 8, 16 and 24 h) after restoring  $\text{Ca}^{2+}$ . Cells were then processed for routine ZO-1 immunofluorescent staining.

**Quantitative reverse-transcriptase (RT)-PCR and qPCR.** Total RNA was extracted from cells using TRIzol (Sigma). cDNA was synthesized using iScript cDNA Synthesis Kit (Bio-Rad, Hercules, CA). qPCRs were performed using SYBR Green supermixture (Bio-Rad) on CFX96 RT-PCR detection system (Bio-Rad). The primers were designed cross two exons to prevent amplification of genomic DNA. Primer sequences and their respective PCR fragment lengths were as follows: CDX2 (122 bp): 5'-CTCGGCAGCCAAGTAAAACCA-3', and 5'-GCTTTCCTCCGGATGGTGATGA-3'; qPCR quantification of CDX2 promoter fragments from chromatin immunoprecipitation (ChIP) for H3K4me3 and H3K27me3 was conducted using CDX2-ChIP (human) (268 bp): forward 5'-GTGGGAGGAAAGAAGGAAGAAAGG-3', and reverse 5'-GTACATGCTCAGTCCTTGCCAG-3'; qPCR quantification of CDX2 promoter fragments from ChIP for EZH2 and LSD1 was conducted using CDX2-ChIP (human) (179 bp): forward 5'-TGCGCCTCGACGTCTCCAAC-3', and reverse 5'-CCTCCCTTCTCTCTTCTTCTCC-3'. qPCR quantification of mouse CDX2 promoter fragments from ChIP for H3K4me3, H3K27me3, EZH2 and LSD1 was conducted using CDX2-ChIP (mouse) (270 bp): 5'-GGTGGTGGTGGGACTGTGTG-3', and reverse 5'-TGCTCCGTCGGCTCTTGC-3'.  $\beta$ -actin was used as an internal control as previously reported.<sup>55</sup>

**Chromatin immunoprecipitation.** Chromatin immunoprecipitation was performed as previously described.<sup>56</sup> Briefly, Caco-2 cells were seeded onto 12-well plates at  $2 \times 10^5$  cells per well for 4 days, cross-linked with 1% formaldehyde for 10 min at room temperature and quenched with 125 mM glycine. After centrifuge, the pellet was lysed in ice-cold lysis buffer with protease inhibitor cocktail (Thermo Fisher Scientific, Waltham, MA, USA), sonicated to break up DNA into 500–800 bp fragments. DNA-protein complex was precleaned with ChIP-grade protein G (Thermo Fisher Scientific), then incubated with an antibody against H3K4me3 (Cell Signaling Technology), H3K27me3 (Cell Signaling Technology), EZH2 (Cell Signaling Technology), LSD1 (Cell Signaling Technology) or normal rabbit IgG (Cell Signaling Technology) overnight at 4 °C. The complex was pulled down with protein G, treated with RNase A (Thermo Fisher Scientific) and proteinase K (Zymo research, Irvine, CA, USA). DNA was purified with ChIP DNA clean and concentrator kit (Zymo Research), and used as templates for qPCR. Relative enrichment of detected proteins was normalized to input DNA using the  $\Delta\Delta\text{-Ct}$  method.

**Transmission electron microscopy.** TEM was performed per previous published method.<sup>57</sup> Briefly, jejunum segments were fixed in McDowell and Trump fixative (VWR, Radnor, PA, USA), rinsed in 0.1 M cacodylate–0.1 M sucrose buffer for En Bloc staining, followed by dehydration. Tissues were infiltrated and embedded in Spurr's low viscosity resin, followed by polymerization for 8 h at 70 °C. Semithin sections were cut using glass knives, and examined under FEI Technai G2 20 Twin TEM (Hillsboro, OR, USA).

**Statistical analysis.** Statistical analyses were conducted as previously described.<sup>58</sup> For cell related studies, at least three independent experiments were carried out. For animal studies, each animal was considered as an experimental unit. Data are presented as means  $\pm$  S.E.M. Statistical analysis was performed using Prism 6 (GraphPad Software, Inc., La Jolla, CA, USA). Differences between means were determined using Student's *t*-test followed by Duncan's multiple test when appropriate.  $P \leq 0.05$  was considered to be statistically significant.

## Conflict of Interest

The authors declare no conflict of interest.

**Acknowledgements.** This work was financially supported by NIH15HD073864. We thank Yansong Xue, Yifei Kang, Shima Bibi and Dr Shuming Zhang for assistance in mice studies, and Dr Xing Fu for valuable discussion of the data interpretation.

- van der Flier LG, Clevers H. Stem cells, self-renewal, and differentiation in the intestinal epithelium. *Annu Rev Physiol* 2009; **71**: 241–260.
- Turner JR. Intestinal mucosal barrier function in health and disease. *Nat Rev Immunol* 2009; **9**: 799–809.
- Hardie DG. AMP-activated/SNF1 protein kinases: conserved guardians of cellular energy. *Nat Rev Mol Cell Biol* 2007; **8**: 774–785.
- Viollet B, Horman S, Leclerc J, Lantier L, Foretz M, Billaud M et al. AMPK inhibition in health and disease. *Crit Rev Biochem Mol Biol* 2010; **45**: 276–295.
- Meddings J. The significance of the gut barrier in disease. *Gut* 2008; **57**: 438–440.
- Peng L, Li Z-R, Green RS, Holzman IR, Lin J. Butyrate enhances the intestinal barrier by facilitating tight junction assembly via activation of AMP-activated protein kinase in Caco-2 cell monolayers. *J Nutr* 2009; **139**: 1619–1625.
- Walker J, Jijon H, Diaz H, Salehi P, Churchill T, Madsen K. 5-aminoimidazole-4-carboxamide riboside (AICAR) enhances GLUT2-dependent jejunal glucose transport: a possible role for AMPK. *Biochem J* 2005; **385**: 485–491.
- Beck F, Chawengsaksohak K, Waring P, Playford RJ, Furness JB. Reprogramming of intestinal differentiation and intercalary regeneration in Cdx2 mutant mice. *Proc Natl Acad Sci USA* 1999; **96**: 7318–7323.
- Berger SL. The complex language of chromatin regulation during transcription. *Nature* 2007; **447**: 407–412.
- Aloia L, Di Stefano B, Di Croce L. Polycomb complexes in stem cells and embryonic development. *Development* 2013; **140**: 2525–2534.
- Eissenberg JC, Shilatifard A. Histone H3 lysine 4 (H3K4) methylation in development and differentiation. *Dev Biol* 2010; **339**: 240–249.
- Mikkelsen TS, Ku M, Jaffe DB, Issac B, Lieberman E, Giannoukos G et al. Genome-wide maps of chromatin state in pluripotent and lineage-committed cells. *Nature* 2007; **448**: 553–560.
- Keating ST, El-Osta A. Epigenetics and metabolism. *Circ Res* 2015; **116**: 715–736.
- Shi X, Wu Y, Ai Z, Liu X, Yang L, Du J et al. AICAR sustains J1 mouse embryonic stem cell self-renewal and pluripotency by regulating transcription factor and epigenetic modulator expression. *Cell Physiol Biochem* 2013; **32**: 459–475.
- Lien F, Berthier A, Bouchaert E, Gheeraert C, Alexandre J, Porez G et al. Metformin interferes with bile acid homeostasis through AMPK-FXR crosstalk. *J Clin Invest* 2014; **124**: 1037.
- Goldberg RF, Austen WG, Zhang X, Munene G, Mostafa G, Biswas S et al. Intestinal alkaline phosphatase is a gut mucosal defense factor maintained by enteral nutrition. *Proc Natl Acad Sci USA* 2008; **105**: 3551–3556.
- Longnus SL, Wambolt RB, Parsons HL, Brownsey RW, Allard MF. 5-Aminoimidazole-4-carboxamide 1- $\beta$ -D-ribofuranoside (AICAR) stimulates myocardial glycogenolysis by allosteric mechanisms. *J Physiol Regul Integr Comp Physiol* 2003; **284**: R936–R944.
- Fournier ML, Paulson A, Pavelka N, Mosley AL, Gaudenz K, Bradford WD et al. Delayed correlation of mRNA and protein expression in rapamycin-treated cells and a role for Ggc1 in cellular sensitivity to rapamycin. *Mol Cell Proteomics* 2010; **9**: 271–284.
- Maloy KJ, Powrie F. Intestinal homeostasis and its breakdown in inflammatory bowel disease. *Nature* 2011; **474**: 298–306.
- Clevers H, Battle E. SnapShot: the intestinal crypt. *Cell* 2013; **152**: e1192.
- Ubelmann F, Chamailard M, El-Marjou F, Simon A, Netter J, Vignjevic D et al. Enterocyte loss of polarity and gut wound healing rely upon the F-actin-severing function of villin. *Proc Natl Acad Sci USA* 2013; **110**: E1380–E1389.
- Bai A, Ma AG, Yong M, Weiss CR, Ma Y, Guan Q et al. AMPK agonist downregulates innate and adaptive immune responses in TNBS-induced murine acute and relapsing colitis. *Biochem Pharmacol* 2010; **80**: 1708–1717.
- Arrieta M, Bistriz L, Meddings J. Alterations in intestinal permeability. *Gut* 2006; **55**: 1512–1520.
- Sciarretta S, Zhai P, Shao D, Maejima Y, Robbins J, Volpe M et al. Rheb is a critical regulator of autophagy during myocardial ischemia pathophysiological implications in obesity and metabolic syndrome. *Circulation* 2012; **125**: 1134–1146.
- Spruss A, Kanuri G, Stahl C, Bischoff SC, Berghelm I. Metformin protects against the development of fructose-induced steatosis in mice: role of the intestinal barrier function. *Lab Invest* 2012; **92**: 1020–1032.
- Xue Y, Zhang H, Sun X, Zhu M-J. Metformin improves ileal epithelial barrier function in interleukin-10 deficient mice. *PLoS ONE* 2016; **11**: e0168670.
- Harmel E, Grenier E, Bendjoudi Ouadda A, El Chebly M, Ziv E, Beaulieu JF et al. AMPK in the small intestine in normal and pathophysiological conditions. *Endocrinology* 2014; **155**: 873–888.
- Cephas KD. Effects of fructan source and degree of polymerization on intestinal barrier function and histomorphology characteristics in obese C57BL/6 mice. MSc thesis, University of Illinois at Urbana-Champaign, Champaign, IL, USA, 2012.

29. Yang G, Wang H, Kang Y, Zhu M. Grape Seed Extract Improves Epithelial Structure and Suppresses Inflammation in the Ileum of IL-10-Deficient Mice. *Food Funct* 2014; **5**: 2558–2563.
30. Wang B, Yang G, Liang X, Zhu M, Du M. Grape seed extract prevents skeletal muscle wasting in interleukin 10 knockout mice. *BMC Complement Altern Med* 2014; **14**: 162.
31. Winder W, Hardie D. AMP-activated protein kinase, a metabolic master switch: possible roles in type 2 diabetes. *Am J Physiol Endocrinol Metab* 1999; **277**: E1–E10.
32. Zheng B, Cantley LC. Regulation of epithelial tight junction assembly and disassembly by AMP-activated protein kinase. *Proc Natl Acad Sci USA* 2007; **104**: 819–822.
33. Fanning AS, Jameson BJ, Jesaitis LA, Anderson JM. The tight junction protein ZO-1 establishes a link between the transmembrane protein occludin and the actin cytoskeleton. *J Biol Chem* 1998; **273**: 29745–29753.
34. Crissey MAS, Guo RJ, Funakoshi S, Kong J, Liu J, Lynch JP. Cdx2 levels modulate intestinal epithelium maturity and Paneth cell development. *Gastroenterology* 2011; **140**: e518.
35. Mallo GV, Soubeyran P, Lissitzky J-C, André F, Farnarier C, Marvaldi J et al. Expression of the Cdx1 and Cdx2 homeotic genes leads to reduced malignancy in colon cancer-derived cells. *J Biol Chem* 1998; **273**: 14030–14036.
36. Gao N, Kaestner KH. Cdx2 regulates endo-lysosomal function and epithelial cell polarity. *Genes Dev* 2010; **24**: 1295–1305.
37. Xie Y, Awonuga A, Liu J, Rings E, Puscheck EE, Rappolee DA. Stress induces AMPK-dependent loss of potency factors Id2 and Cdx2 in early embryos and stem cells. *Stem Cells Dev* 2013; **22**: 1564–1575.
38. Bonhomme C, Duluc I, Martin E, Chawengsaksophak K, Chenard N, Kedinger M et al. The Cdx2 homeobox gene has a tumour suppressor function in the distal colon in addition to a homeotic role during gut development. *Gut* 2003; **52**: 1465–1471.
39. Boyd M, Hansen M, Jensen TG, Pereaunau A, Olsen AK, Bram LL et al. Genome-wide analysis of CDX2 binding in intestinal epithelial cells (Caco-2). *J Biol Chem* 2010; **285**: 25115–25125.
40. Escaffit F, Paré F, Gauthier R, Rivard N, Boudreau F, Beaulieu J-F. Cdx2 modulates proliferation in normal human intestinal epithelial crypt cells. *Biochem Biophys Res Commun* 2006; **342**: 66–72.
41. Meissner A, Mikkelsen TS, Gu H, Wernig M, Hanna J, Sivachenko A et al. Genome-scale DNA methylation maps of pluripotent and differentiated cells. *Nature* 2008; **454**: 766–770.
42. Knutson SK, Wigle TJ, Warholc NM, Sneeringer CJ, Allain CJ, Klaus CR et al. A selective inhibitor of EZH2 blocks H3K27 methylation and kills mutant lymphoma cells. *Nat Chem Biol* 2012; **8**: 890–896.
43. Leeb M, Pasini D, Novatchkova M, Jaritz M, Helin K, Wutz A. Polycomb complexes act redundantly to repress genomic repeats and genes. *Genes Dev* 2010; **24**: 265–276.
44. Adamo A, Sesé B, Boue S, Castaño J, Paramonov I, Barrero MJ et al. LSD1 regulates the balance between self-renewal and differentiation in human embryonic stem cells. *Nat Cell Biol* 2011; **13**: 652–659.
45. Zhu D, Hölz S, Metzger E, Pavlovic M, Jandausch A, Jilg C et al. Lysine-specific demethylase 1 regulates differentiation onset and migration of trophoblast stem cells. *Nat Commun* 2014; **5**: 3174.
46. Laukoetter MG, Nava P, Lee WY, Severson EA, Capaldo CT, Babbin BA et al. JAM-A regulates permeability and inflammation in the intestine in vivo. *J Exp Med* 2007; **204**: 3067–3076.
47. Bu H-F, Zuo X-L, Wang X, Ensslin MA, Koti V, Hsueh W et al. Milk fat globule-EGF factor 8/lactadherin plays a crucial role in maintenance and repair of murine intestinal epithelium. *J Clin Invest* 2007; **117**: 3673.
48. Wirtz S, Neufert C, Weigmann B, Neurath MF. Chemically induced mouse models of intestinal inflammation. *Nat Protoc* 2007; **2**: 541–546.
49. Zhu MJ, Han B, Tong J, Ma C, Kimzey JM, Underwood KR et al. AMP-activated protein kinase signalling pathways are down regulated and skeletal muscle development impaired in fetuses of obese, over-nourished sheep. *J Physiol* 2008; **586**: 2651–2664.
50. Thanou M, Kotze A, Scharringhausen T, Luessen H, De Boer A, Verhoef J et al. Effect of degree of quaternization of N-trimethyl chitosan chloride for enhanced transport of hydrophilic compounds across intestinal Caco-2 cell monolayers. *J Control Release* 2000; **64**: 15–25.
51. Duizer E, Penninks A, Stenhuis W, Groten J. Comparison of permeability characteristics of the human colonic Caco-2 and rat small intestinal IEC-18 cell lines. *J Control Release* 1997; **49**: 39–49.
52. Fu X, Zhao J-X, Zhu M-J, Foretz M, Viollet B, Dodson MV et al. AMP-activated protein kinase  $\alpha 1$  but not  $\alpha 2$  catalytic subunit potentiates myogenin expression and myogenesis. *Mol Cell Biol* 2013; **33**: 4517–4525.
53. Kang Y, Xue Y, Du M, Zhu M-J. Preventive effects of Goji berry on dextran-sulfate-sodium-induced colitis in mice. *J Nutr Biochem* 2017; **40**: 70–76.
54. Elamin EE, Masclee AA, Dekker J, Pieters H-J, Jonkers DM. Short-chain fatty acids activate AMP-activated protein kinase and ameliorate ethanol-induced intestinal barrier dysfunction in Caco-2 cell monolayers. *J Nutr* 2013; **143**: 1872–1881.
55. Zhu M, Du M, Nathanielsz P, Ford S. Maternal obesity up-regulates inflammatory signaling pathways and enhances cytokine expression in the mid-gestation sheep placenta. *Placenta* 2010; **31**: 387–391.
56. Yang Q-Y, Liang J-F, Rogers CJ, Zhao J-X, Zhu M-J, Du M. Maternal obesity induces epigenetic modifications to facilitate Zfp423 expression and enhance adipogenic differentiation in fetal mice. *Diabetes* 2013; **62**: 3727–3735.
57. Nighot PK, Blikslager AT. CIC-2 regulates mucosal barrier function associated with structural changes to the villus and epithelial tight junction. *Am J Physiol Gastrointest Liver Physiol* 2010; **299**: G449–G456.
58. Zhu MJ, Du M, Nathanielsz PW, Ford SP. Maternal obesity up-regulates inflammatory signaling pathways and enhances cytokine expression in the mid-gestation sheep placenta. *Placenta* 2010; **31**: 387–391.

Supplementary Information accompanies this paper on *Cell Death and Differentiation* website (<http://www.nature.com/cdd>)